International Journal of Modern Physics A

SIMULATION OF THE CBETA 4-PASS FFAG ERL USING FIELD-MAPS - EXCLUSIVELY

F. MÉOT, J.S. BERG, S. BROOKS, D. TRBOJEVIC, N. TSOUPAS
Brookhaven National Laboratory
Upton, NY, USA

J. CRITTENDEN
Cornell University (CLASSE)
Ithaca, NY, USA

The Cornell-BNL Electron Test Accelerator (CBETA), a four-pass, 150 MeV energy recovery linac (ERL), is now in construction at Cornell. Commissioning will commence in March 2019. A particularity of CBETA is that a single channel loop recirculates the four energies (42, 78, 114 and 150 MeV). The return loop arcs are based on fixed-field alternating gradient (FFAG) optics. The loop is comprised of 107 quadrupole-doublet cells, built using Halbach permanent magnet technology. Spreader and combiner sections (4 independent beam lines each) connect the 36 MeV linac to the FFAG arcs. We introduce here to a start-to-end simulation of the 4-pass ERL, based entirely, and exclusively, on the use of magnetic field maps to model the optical components.

Keywords: CBETA; FFAG; ERL; Zgoubi.

PACS numbers:

Contents

1. Introduction

The Cornell-BNL Electron Test Accelerator (CBETA),[1] a four-pass, 150 MeV, 40 mA energy recovery linac (ERL), now in construction at Cornell, uses a single channel loop to recirculate four energies, 42, 78, 114 and 150 MeV, four-pass up, four-pass down. The return loop arcs (FA-TA and TB-FB sections, Fig. 1) use fixed-field alternating gradient (FFAG) optics; the straight section (ZA-ZB) is a FoDO

channel with all 4 energies on the common quadrupole axis. The loop is comprised of 107 quadrupole-doublet cells, built using Halbach permanent magnet technology. Spreader (SX) and combiner (RX) sections (4 independent beam lines each) connect the 36 MeV linac to the FFAG arcs, they use conventional electro-magnets. Details regarding CBETA optics can be found in Refs.[1,2]

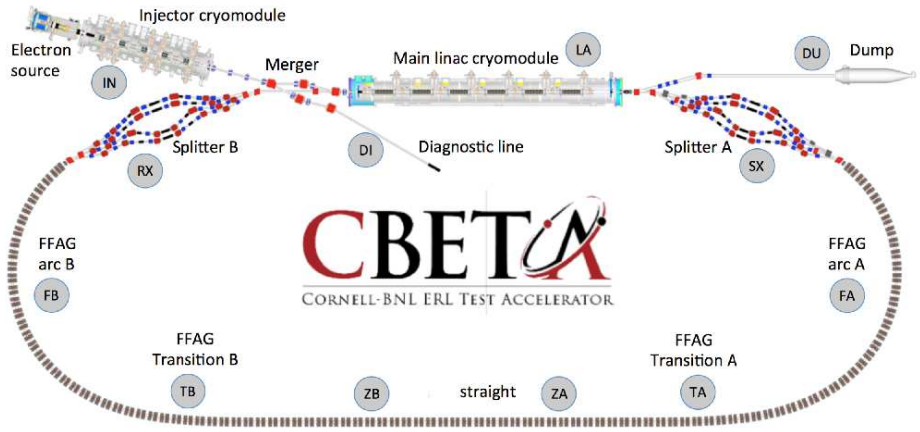

Fig. 1. CBETA 150 MeV ERL. The linac (LA) is 36 MeV, four different energies circulate concurrently in the single-channel return loop (FA-TA-ZA-ZB-TB-FB): 42, 78, 114 and 150 MeV. Four spreader (SX) and recombiner lines (RX), at linac downstream and upstream ends, respectively, ensure proper orbits and optical functions into and out of the return loop.

OPERA field maps of the return loop Halbach magnets have been produced and validated at BNL.[3] OPERA field maps of the spreader and combiner line electromagnets are produced at Cornell.[4] Stepwise ray-tracing results in high simulation accuracy, this is an incentive to using field maps which add to that the accuracy of the field modeling. This may be deemed an advantage in some simulations, for instance beam transport including halo, a critical area at high power ERLs.

On the other hand, a field map based simulation method must be validated, which includes showing the feasibility of

- using separate field maps of the QF, QD and BD quadrupoles and combined function dipoles that make up the return loop,
- accounting for field overlapping between neighboring magnets along the return loop,
- and accounting for dipole corrector windings superimposed on the Halbach magnets.

The interest of using separate field maps is in the flexibility in the modeling, allowing in particular,

- independent fine-tuning of QF, QD and BD Halbach magnet strengths,
- an independent power-supply knob for each corrector,

- the possibility of independent field and positioning errors and compensation,
- easier optical connection between the CBETA sectors (FA, TA, ZA, etc., Fig. 1).

A model of a preliminary 1-pass ER, using these field maps, is discussed here. It will be used for off-line beam dynamics simulations during CBETA commissioning which will commence in March 2019 with a 1-pass ER including 6 MeV linac injection, followed by 42 MeV recirculation, energy recovery down to 6 MeV in the linac, and beam dump. The commissioning of the 4 pass ER will be staged over the coming 2019-2020 period, the field map based simulations will be extended accordingly.

The spectrometer computer code Zgoubi, well equipped and long proven for this type of simulations[5] (CBETA is a time-of-flight spectrometer), including ER,[6,7] and including stepwise ray-tracing in RF cavities, is used for these studies. Note that the code is under development at Radiasoft,[8] which includes its installation in the SIREPO user environment where a model CBETA is being installed.[9]

2. OPERA simulation of CBETA Halbach cells

A brief overview of the field map method and its outcomes is given here. This is a work in progress, the objective being to have in a first stage a complete simulation ready for the 1-pass (42 MeV) energy-recovery commissioning. Note that the permanent magnet channel sequence (FA-FB) only requires a single model which has the virtue of mapping all 4 energies (see Sec. 4), thus a much reduced length of beam lines is left to simulate, once a 1-pass model is in place. Namely (Fig. 1), the remaining three spreader lines (78, 114 and 150 MeV) in the SX section and the three combiner lines (RX section).

The arc proper and the curved dispersion suppression sections (FA, TA and their symmetric TB, FB, Fig. 1) are comprised of FFAG cells, namely, the two Halbach magnets (Figs. 2, 3) act as combined function dipoles. QF is a pure quadrupole in which the orbits at the 4 design energies are off-axis, so contributing a net curvature, BD is a combined dipole+quadrupole structure.

Figure 4 shows a scan in energy of the orbits across the FA and FB arc cell, and the 42 MeV optical functions, obtained using the OPERA field maps of the QF and BD Halbach magnets.

The transition sections TA and TB use the same QF magnet, and two specific BD structures. These focusing and defocusing magnets are slowly shifted with respect to one another along the line, in order to slowly cancel the dispersion prior to connecting to the straight section ZA-ZB.[2] The latter is comprised of pure quadrupole doublet QF+QD cells.

3. Beam optics from field maps

This section shows that the permanent magnet cells can be simulated using independent fields maps of each of the two constitutive magnets, with quasi identical paraxial optics to using a single field map encompassing the two magnets, and very

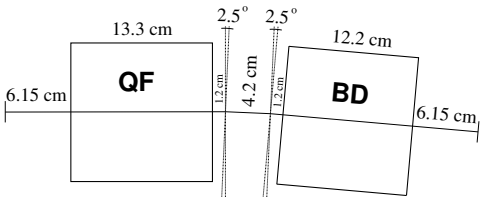

Fig. 2. A sketch of the QF-BD FFAG cell in the FA and FB arcs (Fig. 1). The cell length is 44.4 cm.

An OPERA model is shown in Fig. 3.

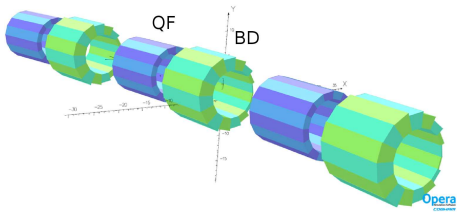

Fig. 3. OPERA model for a single field map of a complete QF-BD cell. The field map is extracted out of a 3-cell series as shown here, in order to ensure periodicity of the field. The present study shows that separate field maps instead, from isolated QF and BD magnets, yield similar beam dynamics.

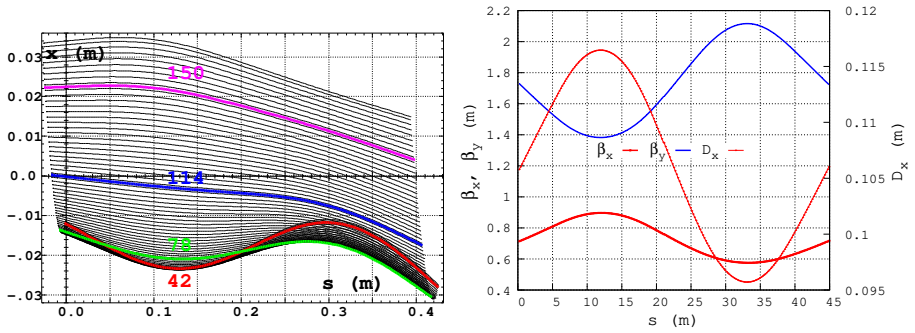

Fig. 4. Using field maps of the Halbach magnets. Left: an energy scan of the orbits across the arc cell, the 4 design energies are the thicker, colored lines. Right: the 42 MeV betatron functions (left axis) and horizontal dispersion (right axis).

similar large excursion dynamics. This is critical to the flexibility of the beam line optics tuning, and to the independent setting of the dipole correctors.

The section also discusses the field map model of the dipole magnets in the SX and RX lines, including practical aspects of the extended fringe fields (a consequence of a substantial bore/length ratio).

3.1. *Halbach cell*

1- First order parameters of the arc cell are displayed in Figs. 6. Table 1 details the path length at the four design energies, depending on the field map modeling method. Differences do not exceed a few ppm.

2- Dynamical admittance at a given energy is defined here as the maximum stable invariant that makes it through a 400 cell channel, for that energy (a particle

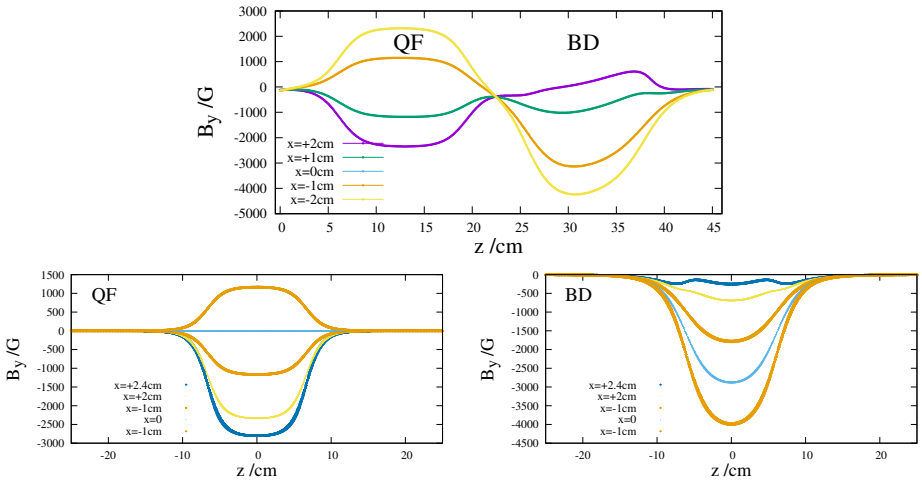

Fig. 5. Top: mid-plane field across the central doublet cell of Fig. 3, samples taken at various distances parallel to the optical axis. Bottom: mid-plane field across the magnets, at various distances parallel to the bore axis, case of separate computation of the two QF and BD field maps.

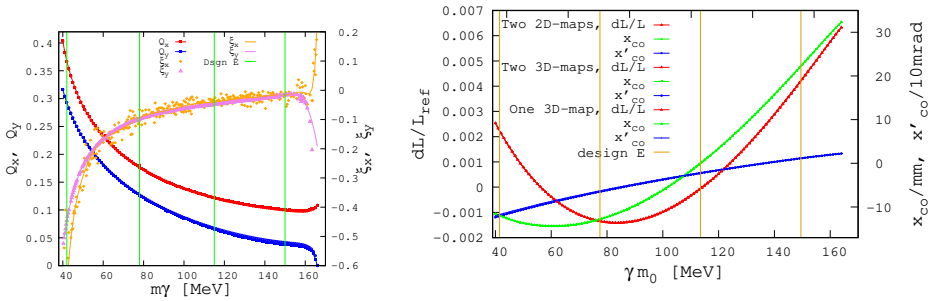

Fig. 6. Separate 2-D or 3-D field maps of QF and BD, or a 3-D full-cell single map, yield, left): same paraxial tunes (left vertical axis) and chromaticities (right axis); right: the same closed orbit coordinates (observed here at the center of the long drift), and the same trajectory lengthening, all superimposed on this graph.

with larger invariant would be kicked away under the effect of field or kinematic non-linearities). The maximum stable invariants so obtained, at each of the four design energies, are displayed in Fig. 7. The admittance is taken as the surface encompassed within the invariant boundary.

The previous exercise is repeated for a series of energies ranging from 39 to 170 MeV. The resulting energy scans are shown in Fig. 8 for three different cases of field map based modeling: using separate QF, BD (i) 2-D or(ii) 3-D maps; (iii) using a single 3-D map. It can be noted in passing that the cell design has placed the 42 MeV beam away from the Walkinshaw resonance (the dip in the vertical accep-

Case of separate QF and BD 2-D field maps:

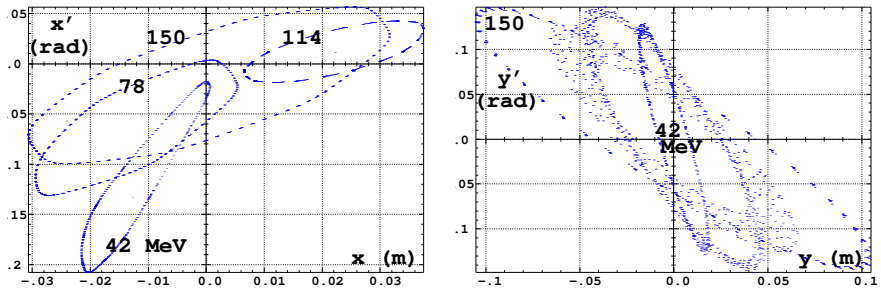

Case of single full-cell 3-D field map:

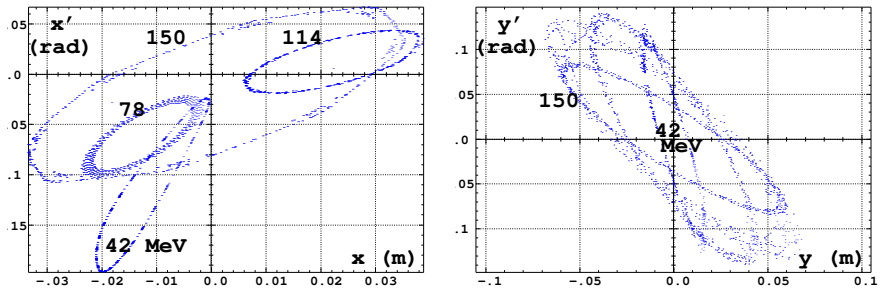

Fig. 7. Left column: horizontal motion; right column: vertical motion. Observation plane is at the middle of the long drift. Non-linearities at the origin of the limited amplitude are from the field and from motion kinematic terms. The maximum invariant values, normalized, are in the meter range and remain similar whether two separate 2-D or 3-D field maps or a single full-cell 3-D map is used to model the doublet cell. Note that these invariant values are far beyond the μ**m** normalized CBETA beam emittance.

tance, to the left of the 42 MeV vertical bar), and from the $Q_x = 1/3$ resonance (the dip in the horizontal acceptance, to its right).

3- Outcomes. The DA curves in the three models superimpose reasonably: all three yield comparable admittances (centimeters to meter, normalized), *a fortiori* they indicate that comparable transverse motion will result, up to amplitudes that exceed by far CBETA beam emittances (in the μm range, normalized). This justifies using independent field maps of the magnets (field profiles as in the two Figs. 5-bottom), in lieu of longer field maps covering two magnets or more (field profile as in Fig. 5-top). An additional outcome is that 2-D field maps yield convenient motion integration accuracy, no need of 3-D maps - but for halo studies perhaps, this needs be investigated.

A complete cell model as simulated in these studies is shown in Fig. 9. The model includes the horizontal and vertical orbit correction dipoles on top of respectively the F and D Halbach magnets. This requires two independent additional field maps

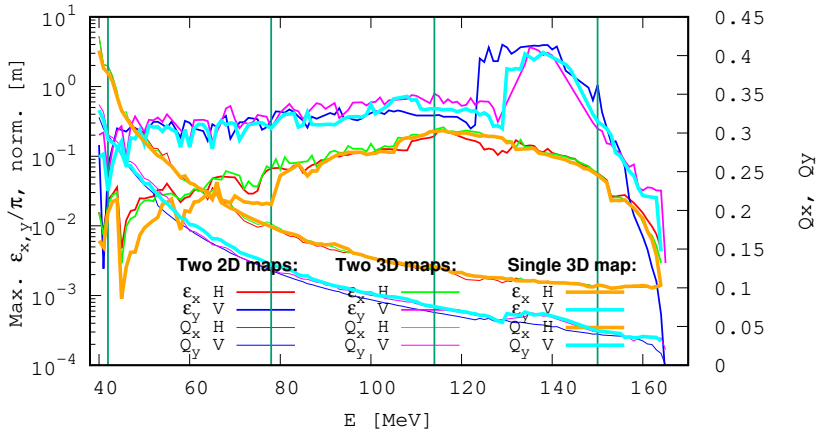

Fig. 8. Energy dependence of the 400-cell dynamical acceptance of the Halbach arc cell (left vertical scale), in three cases of field map based modeling: using separate QF and BD (i) 2-D maps; (ii) 3-D maps; or (iii) using a single QF-BD 3-D map. "H" designates horizontal motion (initial V invariant is taken very small), "V" designates vertical motion (initial H invariant is taken very small). The cell tunes (right scale) are for the maximum invariants, computed using a discrete Fourier transform.

in order to allow two independent knobs. Note that in the case of a full-cell single field map, as was done for the EMMA FFAG ring,[10] these two additional field maps are designed in the following manner:

- the F-corrector map has the F-corrector on and the D-corrector off,
- the D-corrector map has the F-corrector off and the D-corrector on.

For the sake of clarity regarding the practical handling of the various field maps, the arc cell sequence below shows how the input data list to Zgoubi appears in the case of separate F-magnet and D-magnet field maps, when including field maps of all magnetic components (details regarding the handling and functioning of the optical keywords proper, can be found in the users' guide of the code[5]).

• Focusing magnet & corrector:

```
'TOSCA'   ! A keyword that causes integration through field map
0 0
-9.699E-04 1. 1. 1. ! Field & coordinates normalization.
HEADER_8  ZroBXY
501 83 1 15.2  1. 0.     ! Two field map tuning factors.
QF-2D-fieldMap.table     ! QF OPERA map,
FCorr-2D-fieldMap.table  ! F-corfrector map.
0 0 0 0
2
.1           ! integration step size (cm).
2 0. 0. 0.    ! Magnet positionnng.
```

• Defocusing magnet & corrector:

```
'TOSCA'
0  0
 -9.699E-04  1.  1.  1.
HEADER_8  ZroBXY
501 83 1  15.1  1.0      ! Two field map tuning factors.
BD-2D-fieldMap.table     ! BD OPERA map,
DCorr-2D-fieldMap.table  ! D-corfrector map.
0 0 0 0
2
.1           ! integration step size (cm).
2 0. 0. 0.    ! Magnet positionnng.
```

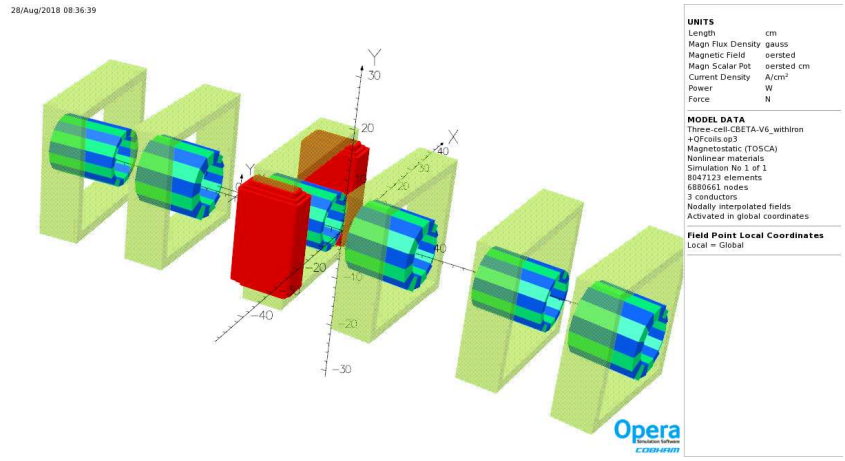

Fig. 9. A 3-cell OPERA simulation, including horizontal and vertical orbit corrector dipoles (iron yoke electromagnets), on top of respectively the focusing and defocusing Halbach magnet (red: the sole QF corrector is highlighted here).

3.2. *SX and RX magnets*

Changing the modeling of the dipoles and quadrupoles in the SX and RX lines, from regular first order mapping to using field maps, results in weak changes in the orbit geometry and length, and in the first order transport coefficients. This is due for part to the gap/length aspect ratio of the magnets, which is not on the small side with a gap of 3.6 cm and dipole lengths of 7 to 20 cm. The cumulative effect over the extent of an SX or RX line, which counts about 10 dipoles (all rectangular), is sensible.

A typical example of the various ways to model the field in an SX or RX dipole, and the resulting effect on the first order transport coefficients and path lengths, is given in Fig. 10. In the case (ii) of a pure dipole with extended field fall-offs, two parameters had to be varied in order to get R_{21} and R_{43} transport coefficient values comparable to the (iii) OPERA model ones, namely, a/ the fall-off extent and b/ departure from a rectangular magnet. The latter amounts to a 6^o parallelism defect of that 18^o dipole effective field boundaries.

Details regarding the design of the SX and RX line magnets can be found in Ref.[4]

4. A simulation of the 42 MeV, 1-pass ER lattice (sample)

CBETA commissioning will start with that configuration: single-pass, 36 MeV energy recovery, beam dump. Excerpts from simulations regarding the optics along the various sections of the return loop are briefly discussed here.

Fig. 11 shows the optical functions from Zgoubi and from Cornell's BMAD model of the CBETA lattice;[11] the orbits along S1 and R1 have been set to zero by prior

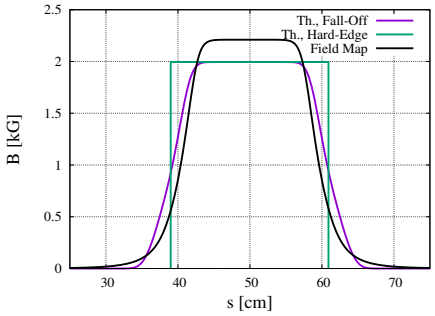

Fig. 10. Field along the reference orbit across one typical dipole of the SX or RX beam lines. Three different field models are ray-traced: (i) hard edge; (ii) pure dipole field with field fall-offs; (ii) OPERA field map of the dipole. The field integral ($\int \mathrm{B(s)}\,\mathrm{ds} = 0.044\,\mathrm{T\,m}$ in this particular dipole) is the same in all 3 models.

([$\mathrm{R_{i=1-4,5;j=1-4,6}}$]) transport matrix from (i) hard-edge model for reference; (ii) pure dipole field with fringe fields; (iii) OPERA model:

```
(i) Hard-edge.  Arc length: 22.0606 cm
 1          0.216997    0           0          -3.436E-02
 0           1          0           0          -0.316659
 0           0          0.950276    0.220605   0
 0           0         -0.439585    0.950276   0
-0.31666    -0.034357   0           0          3.6085E-03

(ii) Fringe field.  Arc length: 22.0511 cm
 0.98493     0.216780   0           0          -3.433E-02
-0.13788     0.984953   0           0          -0.314304
 0           0          0.97108     0.220804   -0
 0           0         -0.258899    0.970985   0
-0.31430    -0.034326   0           0          3.7942E-03

(iii) OPERA map.  Arc length: 21.9227 cm
 0.983444    0.215709   0           0          -3.4153E-02
-0.151999    0.983583   0           0          -0.314091
 0           0          0.969607    0.218802   0
 0           0         -0.273559    0.969615   0
-0.314079   -0.0341572  0           0          3.60475E-03
```

proper scaling of each one of the dipole field map fields to yield design bending. Fig. 12 shows the orbits at the four design energies along the FA to FB permanent magnet return loop. The orbits start from the upstream end of the FA arc with their theoretical orbit coordinates there, and proceed freely without any orbit correction applied, all the way down to the end of FB arc; a minor wiggling of the orbits is observed along the TB and FB sections, and at 42 MeV in the ZA-ZB straight, which can be fixed with minor orbit correction. Fig. 12-right details the 42 MeV orbit freely propagating from S1 to R1 included, essentially ready for the CBETA commissioning studies to come. Fig. 13-left shows the 42 MeV betatron functions along the first meters of the FA section. Fig. 13-right shows the betatron functions along R1 after propagating freely from S1 to R1, with merely their initial values imposed at the exit of the linac (S1 is set as shown in Fig. 11-left). All these results obtained using exclusively the OPERA field maps of the magnets.

Linac

The linac is not discussed here, as it is not relevant to the question of using magnetic field maps. It is not considered a difficulty anyway, as start-to-end energy recovery simulations have been realized regarding much larger scale installations, for instance, a 1-pass 1.4 GeV ER in CEBAF with each of its two linacs set to 700 MeV;[7] a 12-pass up/12-pass down ER in a model of the linac-ring Electron-Ion Collider studied at BNL in the recent years, which is based on a 120 long, 1.3 GeV linac and a 3.8 km multiple-beam FFAG return channel.[6]

On the other end, it is foreseen to use electro-magnetic field maps of the CBETA 36 MeV linac RF cavities to improve the simulations. This will subject to future developments in the present field map based model in Zgoubi.

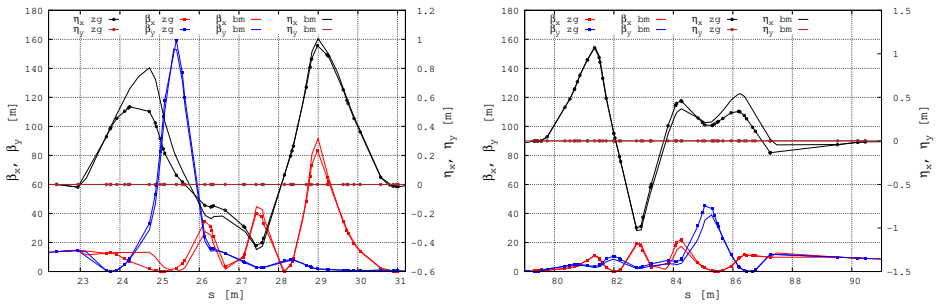

Fig. 11. S1 (left) and R1 (right) optics, using field maps for all dipoles, after re-match of the downstream optical functions to the entrance of the FFAG loop. Left vertical axis: betatron functions; right axis: horizontal dispersion (η_y is null). Incoming optical functions are taken from linac exit. Data from Cornell's BMAD model (bm, thin lines) are shown for comparison.

5. In conclusion

The field map based simulations of CBETA discussed here show that accurate bunch tracking is to be expected from that method. This tool will be used, off-line, as part of CBETA commissioning. It can further serve for beam halo studies, which requires tracking accuracy.

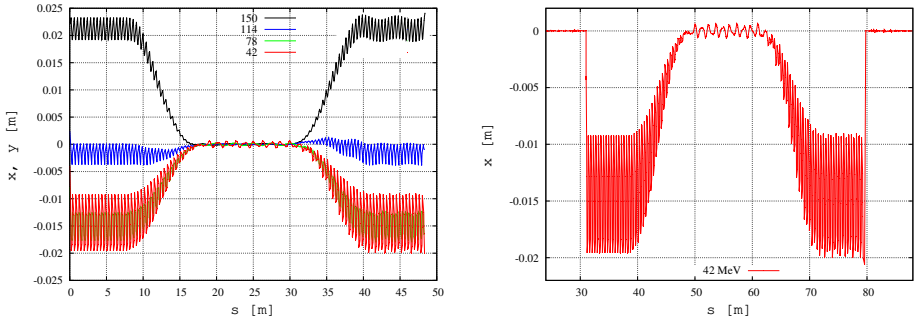

Fig. 12. Left: 42, 78, 114 and 150 MeV orbits along the FA-FB section of the return loop, freely propagating, without any correction, from their initial theoretical value at the start of the FA arc. Right: details of the 42 MeV orbit, including S1 and R1.

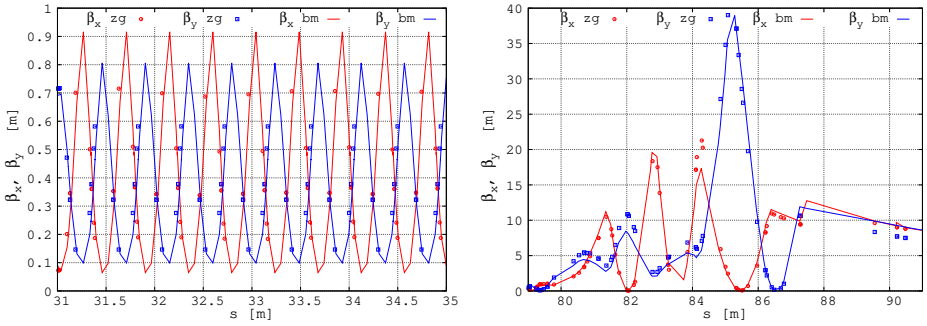

Fig. 13. Betatron functions at 42 MeV. Left: along the first meters of the FA section. Right: along R1 after propagating freely from S1 to R1, with merely their initial values imposed at the exit of the linac (optics in S1 as shown in Fig. 11-left); comparison with Fig. 11-right shows some difference when theoretical initial values (that at FB end) are imposed at start of R1: minor retuning will be sufficient to take care of the departure observed and of matched values to linac entrance. Markers: records from field map simulations. Thin lines: from Cornell's BMAD model for comparison.

Table 1. Path lengths in the different field map models. The cell length is 44.4 cm (Fig. 2).

E (MeV)	42	78	114	150
Case of single 3-D map	44.4846	44.3298	44.3898	44.5806
Case of two maps (2-D or 3-D)	44.4845	44.3291	44.3884	44.5797

References

1. J. Barley et als., CBETA Design Report, Jan. 27, 2017. https://app.box.com/file/116481645496.
2. J.S. Berg et als., CBETA FFAG Beam Optics Design, Proc. ERL17 Conf., http://accelconf.web.cern.ch/AccelConf/erl2017/papers/tuidcc004.pdf.
3. F. Méot et als., Beam dynamics validation of the Halbach Technology FFAG Cell for Cornell-BNL Energy Recovery Linac, *NIM A* **896** (2018) 60-67.
4. J.A. Crittenden et als., Magnet design for the splitter/combiner regions of CBETA, the Cornell-BNL energy-recovery-linac test accelerator, MOPOB59, Proc. NAPAC16 Conf. (2016).
5. https://zgoubi.sourceforge.io/ZGOUBI_DOCS/Zgoubi.pdf; https://www.osti.gov/scitech/biblio/1062013-zgoubi-users-guide.
6. F. Méot et als., eRHIC ERL modeling in Zgoubi, eRHIC Note 49 (2016); https://technotes.bnl.gov/PDF?publicationId=38865.
7. F. Méot, Y. Roblin, ER@CEBAF: Modeling code developments, eRHIC Note 52 (2016); https://technotes.bnl.gov/PDF?publicationId=40142.
8. D. Abell, "Zgoubi: Recent Developments and Future Plans", *Proc. ICAP18 Conf.*, Key West (2018)
9. P. Moeller, Radiasoft, priv. comm., Oct. 2018. An interface to accelerator codes, https://beta.SIREPO.com/#/accel.
10. Y. Giboudot, F. Méot, Optical matching of EMMA cell parameters using field map sets, *Proc. PAC09*, Vancouver, BC, Canada, TH5PFP040.
11. W. Lou et als., Start to End Simulation of the CBETA Energy Recovery Linac, Proc IPAC18 Conf., Vancouver; http://accelconf.web.cern.ch/AccelConf/ipac2018/papers/thpaf021.pdf.